



Nonlinearity-induced chiral solitonlike edge states in Chern systems

Motohiko Ezawa 

Department of Applied Physics, University of Tokyo, Hongo 7-3-1, 113-8656, Japan

 (Received 5 January 2022; revised 24 September 2022; accepted 14 November 2022; published 28 November 2022)

We study the nonlinear effect on topological edge states by including a nonlinear term to a Chern insulator which has two chiral edge states with opposite chiralities. We explore quench dynamics by giving a pulse to one site on an edge and by analyzing its time evolution. Without the nonlinearity, an initial pulse spreads symmetrically and diffuses. On the other hand, with the nonlinearity present, unexpectedly a solitonlike edge state is formed, undergoes a unidirectional propagation along the edge, and turns at a corner without backscattering or diffraction. Furthermore, its wave function is well fitted by $\propto \text{sech}[k_x(x - v_x t)]$. A further increase of the nonlinearity induces a self-trapping transition, where the pulse is trapped to the initial site.

DOI: [10.1103/PhysRevB.106.195423](https://doi.org/10.1103/PhysRevB.106.195423)

I. INTRODUCTION

Both topology and nonlinearity continue to be the main topics in the history of physics, which have been mainly studied independently. An interplay between topology and nonlinearity creates a frontier of physics. Indeed, nonlinear topological physics is an emerging field, which is now studied in photonic [1–10], mechanical [11–14], electric circuit [15–17], and resonator [18] systems. The simplest model is the nonlinear Su-Schrieffer-Heeger model [2,6,15,19,20].

A characteristic feature of topological systems is the emergence of topological edge states, which are immune to disorders and randomness in a sample. A nonzero topological number indicates a nontrivial topological structure of the hopping matrix.

A prominent feature of a continuous nonlinear system is a soliton, which is an exact solution describing a wave packet stabilized by the nonlinear interaction. However, a lattice system cannot support solitons due to the Peierls-Nabarro potential [21–24] caused by the discreteness of the system. Solitonlike edge states propagating along a topological edge of a sample are fascinating objects in lattice systems [1,25–27]. An interplay or a competition between topology and nonlinearity is a main issue of nonlinear topological systems.

In this paper, we propose a nonlinearity-induced chiral solitonlike edge state propagating along an edge by analyzing a Chern insulator together with a nonlinear term based on quench dynamics. Quench dynamics provides us with a powerful method to reveal the essence of nonlinear topological systems [8], where a pulse is given to one site on an edge as the initial condition. The time evolution reveals both an interplay and a competition between topology and nonlinearity in the present system.

First, without the nonlinear term, the initial pulse spreads symmetrically around the initial site even in the topological phase. This is because two chiral edge modes with opposite chiralities are present and because the pulse excites bulk sites symmetrically as well. Second, with the nonlinear term, the wave packet moves unidirectionally, because one of the two

chiral edge modes is dominantly excited. Finally, when the nonlinearity is strong enough, a self-trapping transition is induced, where the edge modes are trapped to the initial site and make no motion. However, a much more intriguing phenomenon occurs in the presence of appropriate nonlinearity before the self-trapping transition occurs. Indeed, unexpectedly, a solitary wave is formed and propagates unidirectionally along the edge. The propagation direction is determined by the direction of the gauge flux implicit in the Chern insulator. We call it a nonlinearity-induced chiral solitonlike edge state. The solitonlike state turns at a corner without backscattering or diffraction.

II. MODEL

We investigate a nonlinear Schrödinger equation on a lattice [28–34],

$$i \frac{d\psi_n}{dt} + \kappa \sum_m M_{nm} \psi_m + \xi |\psi_n|^2 \psi_n = 0. \quad (1)$$

This is the Hamilton equation, $id\psi_n/dt = \partial H/\partial \psi_n^*$, with the Hamiltonian

$$H = -\kappa \sum_{n,m} M_{nm} \psi_n^* \psi_m - \sum_n \frac{\xi}{2} |\psi_n|^4 \equiv K + U. \quad (2)$$

The first term is the kinetic energy K while the second term is the potential energy U . The Hamiltonian is a conserved quantity. There is one more conserved quantity,

$$N_{\text{exc}} = \sum_{n=1}^N |\psi_n|^2, \quad (3)$$

which is the excitation number.

III. CHERN INSULATOR

We first study the kinetic term, which involves the hopping matrix M_{nm} and the coupling strength κ . We consider the

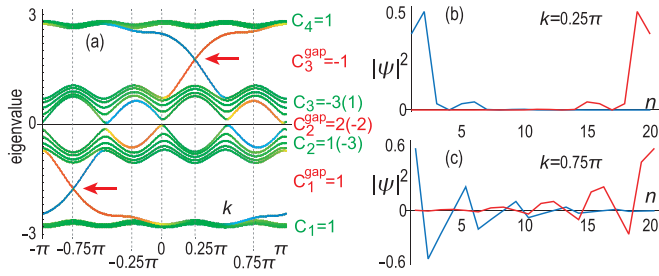


FIG. 1. (a) Band structure of the matrix M_{nm} in nanoribbon geometry. Curves in red (cyan) indicate the localized down (up)-edge states, while those in green indicate the bulk states. The edge state colored in red and pointed by an arrow is right (left) going along the down edge when it has positive (negative) eigenvalue. The band Chern number C_n for the n th band is indicated in green while the gap Chern number C_n^{gap} for the r th gap is indicated in red. The horizontal axis is the momentum k ranging from $-\pi$ to π . The vertical axis is the eigenvalue. The LDOS $|\psi_n|^2$ is shown at (b) $k = 0.25\pi$ and (c) $k = 0.75\pi$. It is localized at the down edge at $n = 1$ and up edge at $n = 20$. The horizontal axis is the lattice site n . The nanoribbon width is $L = 20$.

hopping matrix in the form of

$$M_{nm} = e^{i\alpha n_y} |n_x + 1, n_y\rangle \langle n_x, n_y| + e^{-i\alpha n_y} |n_x, n_y\rangle \langle n_x + 1, n_y| + |n_x, n_y + 1\rangle \langle n_x, n_y| + |n_x, n_y\rangle \langle n_x, n_y + 1|, \quad (4)$$

where $n = (n_x, n_y)$. The system is topological because the hopping matrix Eq. (4) describes the Chern insulator for $\alpha \neq 0, \pi$ or the quantum Hall effect with α representing the penetrated gauge flux into a plaquette of the square lattice. This model is also realized in photonic systems by making coupled resonator optical waveguides [33,35–37], where ψ represents the electric field and α represents a gauge flux in the Landau gauge.

We take $\alpha = \pm\pi/2$ explicitly in what follows. When $\alpha = \pi/2$, we have a four-band model given by

$$M(k_x, k_y) = \begin{pmatrix} 2 \cos k_x & 1 & 0 & e^{-ik_y} \\ 1 & -2 \sin k_x & 1 & 0 \\ 0 & 1 & -2 \cos k_x & 1 \\ e^{ik_y} & 0 & 1 & 2 \sin k_x \end{pmatrix} \quad (5)$$

in the momentum space. When $\alpha = -\pi/2$, we have Eq. (5) with the replacement of k_x by $-k_x$. It means that the sign of α determines the hopping direction.

As a characteristic feature of a Chern insulator, chiral edge states emerge in nanoribbon geometry. The band structure of the matrix κM is shown in Fig. 1(a), where we clearly observe four topological edge states designated by two sets of crossed red and cyan curves. They are two chiral edge modes with positive energy connecting two separate bulk bands at $k = 0.25\pi$ and negative energy at $k = -0.75\pi$, where the direction of the chirality is opposite. In addition, there are two nonchiral edge modes at $k = 0.75\pi$ and $k = -0.25\pi$, which are the slightly

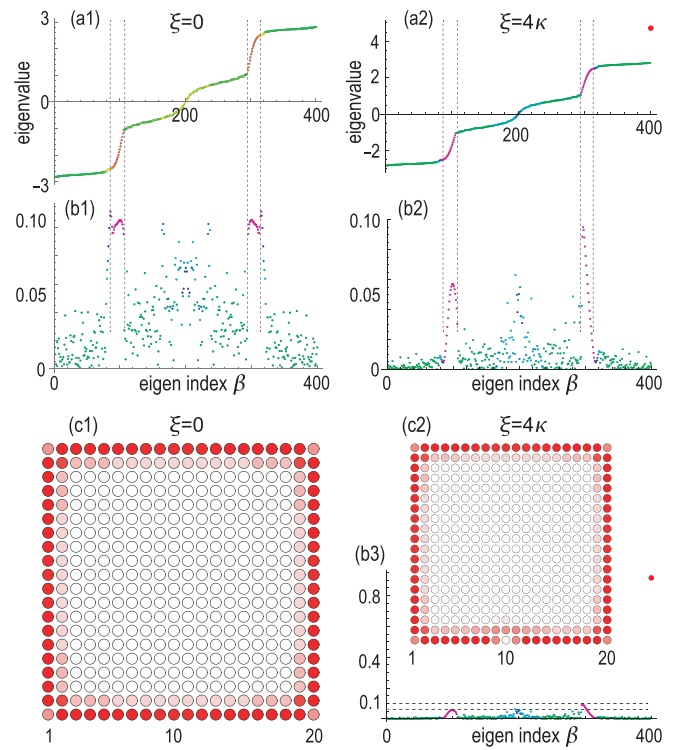


FIG. 2. Eigenspectrum of the matrix M_{nm} in square geometry in (a1) the linear model ($\xi = 0$) and (a2) the nonlinear model ($\xi = 4\kappa$). The mean-field approximation is used for the nonlinear case, and the matrix M_{nm} is evaluated at the initial time with the initial condition Eq. (11). The red parts of a curve indicate the edge states while the green parts indicate the bulk states. The horizontal axis is the eigenindex β of the state $\tilde{\psi}_n^{(\beta)}$, while the vertical axis is the eigenvalue. (b1)–(b3) The component $|c_\beta|^2$ corresponding to the eigenenergy in (a1) and (a2), where (b2) is an enlarged figure of (b3). The red points in (a2) and (b3) represent the isolated eigenmode emerging only in the nonlinear model whose origin is the initial condition imposed in the quench dynamics. Eigenindex β is sorted in the increasing order of E_β . (c1), (c2) The LDOS $|\psi_n|^2$ designated by the strength of red. It is localized along the edges, representing the topological edge modes. In the presence of the nonlinearity, the topological edge state detours the initial point $(n_x, n_y) = (10, 1)$ as in (c2). We have used a square with size 20×20 .

detached ones from the bulk bands. We show the local density of states (LDOS) at $k = 0.25\pi$ and $k = 0.75\pi$ in Figs. 1(b) and 1(c), where there are two edge states localized at the up and down edges.

Next, we calculate the eigenspectrum of the matrix M in square geometry, which is shown in Fig. 2(a1). We also show the LDOS for an edge state in Fig. 2(c1), where the eigenfunction is well localized at the edge of the square and represents a topological edge state.

In the Chern insulator, the Chern number is assigned to each bulk band and the number of chiral edge states corresponds to the difference of the Chern numbers between two adjacent bands. We call this difference as the gap Chern number and the ordinary Chern number as the band Chern number, for clarity, in the following.

The gap Chern number $C_r^{\text{gap}} = t_r$ for the r th gap is determined by the Diophantine equation [38–40],

$$r = qs_r + pt_r, \quad (6)$$

with the flux $\alpha = 2\pi p/q$, where s_r and t_r are integers and $|t_r| \leq q/2$. Here $\alpha = \pi/2$ with $p = 1$ and $q = 4$. Hence, it is explicitly solved as

$$1 = 4s_r + t_r, \quad (s_r, t_r) = (0, 1), \quad (7)$$

$$2 = 4s_r + t_r, \quad (s_r, t_r) = (0, 2), \quad (1, -2), \quad (8)$$

$$3 = 4s_r + t_r, \quad (s_r, t_r) = (1, -1). \quad (9)$$

The Chern number C_1^{gap} for the first gap is 1 as in Eq. (7) and the C_3^{gap} for the last gap is -1 as in Eq. (9), which corresponds to the chiral edge states [41]. On the other hand, when the second and third bands are not separated, the gap and band Chern numbers are not uniquely fixed [40] as in Eq. (8). Indeed, there are two edge states (colored in red and blue) between the second and third bands in Fig. 1(a).

On the other hand, the band Chern number C_n for the n th band is assigned from the relation [38,39,42]

$$C_{n+1} - C_n = C_r^{\text{gap}}, \quad (10)$$

where the r th band gap exists between the n th and $(n+1)$ th bands. They are shown in Fig. 1(a). The Chern numbers for the second and third bands have ambiguity because they are touched at the zero energy [40]. We note that the sum of the Chern number for all bands is zero for the tight-binding model.

IV. QUENCH DYNAMICS

We solve the nonlinear Schrödinger Eq. (1) under the initial condition,

$$\psi_n^{\text{ini}} = \delta_{n_x, L_x/2} \delta_{n_y, 1}, \quad (11)$$

where L_x is the length of the edge along the x axis with L_x an even number. This is the quench dynamics, which has been employed to reveal topological edge states in one dimension [8,10,13,17,43] and topological corner states in two dimensions [8,10]. The hopping term favors the pulse to expand all over the sample, while the nonlinear term favors the pulse to be self-trapped to the initial state. We expect an intriguing phenomenon to occur in the presence of the topological edge state, when these two terms compete among themselves.

First, we study the linear model by setting $\xi = 0$ in Eq. (1). We expand the initial state Eq. (11) by the eigenfunctions

$$\psi_n^{\text{ini}} = \sum_{\beta} c_{\beta} \bar{\psi}_n^{(\beta)}, \quad (12)$$

where $\bar{\psi}_n^{(\beta)}$ is the eigenfunction of the matrix κM_{nm} and β is the index of the eigenenergy:

$$\kappa M_{nm} \bar{\psi}_m^{(\beta)} = E_{\beta} \bar{\psi}_n^{(\beta)}. \quad (13)$$

The square of the component $|c_{\beta}|^2$ is shown in Fig. 2(b1). It has peaks at the edge states colored in red but it also has values in bulk states colored in green.

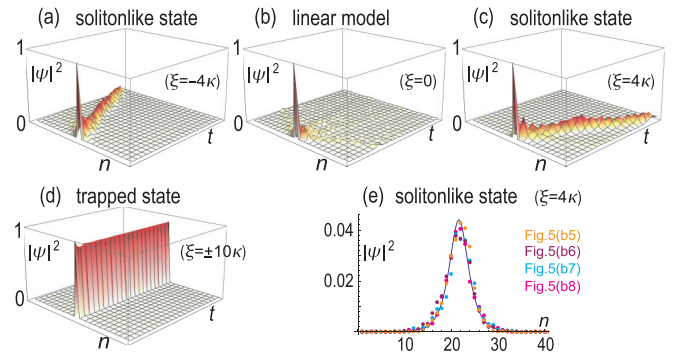


FIG. 3. Time evolution of the LDOS $|\psi_n|^2$ (b) in the linear model ($\xi = 0$), (a) and (c) representing a solitary wave in the nonlinear model ($\xi = \pm 4\kappa$), and (d) representing a trapped wave in a strong nonlinear model ($\xi = \pm 10\kappa$). We have used a square sample with size 20×20 . The horizontal axes are the lattice site n ($1 \leq n \leq 20$) and time t ($0 \leq t \leq 0.5$) in unit of $1/\kappa$. (e) A solitonlike edge state in a rectangular sample with size 500×10 , whose data are extracted from Figs. 6(b5)–6(b8). The solid curve represents the solitary wave function in Eq. (18). Fitting parameters are $A = 0.0455$, $k_x = 0.55$, and $v_x = 0.16$. We have used the initial condition Eq. (11) for all.

We show the time evolution of the amplitude $|\psi_n|^2$ along the edge in Fig. 3 when a pulse is given to site $(L_x/2, 1)$ as an initial condition. It exhibits distinct behaviors depending on ξ . Typical behaviors are as follows. When $\xi = 0$, the localized state rapidly spreads as in Fig. 3(b). On the other hand, when $\xi = \pm 4\kappa$, we observe a solitary wave propagation as in Figs. 3(a) and 3(c). The velocity of the wave packet is opposite for positive and negative nonlinearity ξ . When $\xi = \pm 10\kappa$, the state remains localized as in Fig. 3(d). We explore these characteristic phenomena in more detail.

A. Linear model

The time evolution of the LDOS $|\psi_n|^2$ for the linear model ($\xi = 0$) is shown in Figs. 4(a1)–4(a5). The amplitude spreads not only along the edge but also into the bulk in a symmetric way between the right and left sides. This is because there are two pairs of chiral edge states with opposite chiralities, as shown in Fig. 1(a). In fact, the occupation of these two opposite chiral edge states is identical, as shown in Fig. 2(b1).

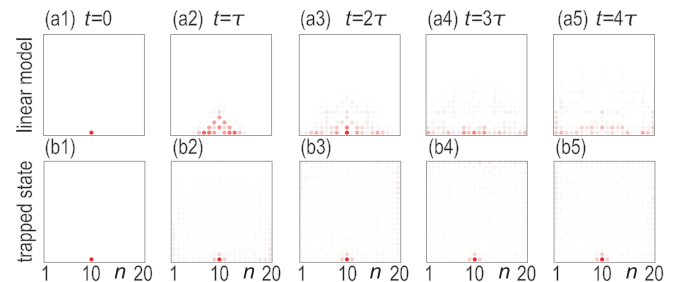


FIG. 4. Time evolution of the spatial profile of the LDOS in a whole square sample with size 20×20 . (a1)–(a5) The LDOS in the linear model with $\xi = 0$, where it diffuses as time passes. (b1)–(b5) The LDOS in a strong nonlinear model with $\xi = 10\kappa$, where it is unchanged as time passes: The time step is $\tau = 2$ in units of $1/\kappa$.

Another feature is that considerable amounts of the amplitude $|\psi_n|^2$ penetrate into the bulk, although we start with the state localized at the edge as in Eq. (11). This is because a pulse excites bulk states as well.

B. Mean-field theory

It is an intriguing phenomenon that a unidirectional solitary wave emerges in the nonlinear model ($\xi \neq 0$). To understand it, we analyze the nonlinear effect in the mean-field approximation. We approximate the nonlinear term as

$$\xi |\psi_n|^2 \psi_n \simeq \xi \langle |\psi_n|^2 \rangle \psi_n, \quad (14)$$

where $\langle |\psi_n|^2 \rangle$ is the expectation value of $|\psi_n|^2$. The Schrödinger Eq. (1) is linearized with the hopping matrix M_{nm} replaced by

$$\tilde{M}_{nm} = M_{nm} + (\xi/\kappa) \langle |\psi_n|^2 \rangle \delta_{nm}. \quad (15)$$

The nonlinearity term acts as an on-site potential. Let us diagonalize Eq. (15) at the initial time, where

$$\langle |\psi_n|^2 \rangle = \delta_{n_x, L_x/2} \delta_{n_y, 1}, \quad (16)$$

with use of the initial condition Eq. (11). We study the case $\xi = 4\kappa$. We show the eigenspectrum in Fig. 2(a2) and $|c_\beta|^2$ in Fig. 2(b3). Figure 2(b2) is an enlarged figure of Fig. 2(b3), where the distribution is clearly asymmetric between the two chiral edge states having positive and negative eigenvalues. The asymmetry corresponds to the asymmetry between the right-going and left-going edge states, leading to a unidirectional motion of the wave packet. Recall that the edge mode is right (left)-going when it has a positive (negative) eigenvalue, as explained in the caption of Fig. 1(a). Hence, the right (left)-going wave-packet motion occurs for $\xi > 0$ ($\xi < 0$).

C. Wave packet

We investigate the wave packet numerically without using the mean-field theory. The mean position $\langle x \rangle$ of the wave packet is given by

$$\langle x \rangle \equiv \sum_{n_x, n_y} (n_x - L_x/2) |\psi_{n_x, n_y}|^2. \quad (17)$$

We calculate the time evolution of $\langle x \rangle$ for various ξ , fit the position by a linear function $\langle x \rangle = v_x t$, and estimate the velocity v_x as a function of ξ , whose result is summarized in Fig. 5(a). The velocity is zero for $\xi = 0$. It linearly increases for $|\xi| \lesssim 4\kappa$, suddenly decreases for $|\xi| \gtrsim 4\kappa$, and makes a jump at $|\xi| \approx 5.6\kappa$.

D. Chiral solitonlike edge state

In the nonlinear model with $\xi = 4\kappa$, the quench dynamics is shown in Figs. 6(a1)–6(a8) for a rectangle with size 80×10 , and in Figs. 6(b1)–6(b8) for a rectangle with size 500×10 , and in Figs. 6(c1)–6(c8) for a square with size 20×20 . A remarkable feature is that the shape of the wave packet remains unchanged beyond 250 sites, as shown in

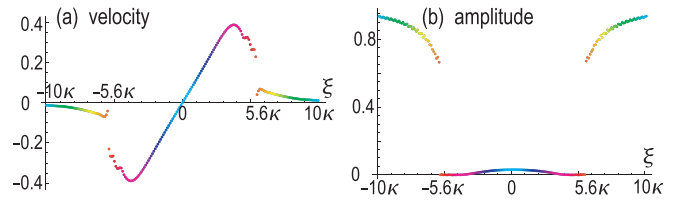


FIG. 5. (a) Velocity v_x as a function of ξ , which is linear for $\xi \gtrsim 4\kappa$. The vertical axis is velocity in unit κ , while the horizontal axis is ξ . (b) Amplitude $|\psi_{L_x/2, 1}|^2$ at the initial point as a function of ξ . Color indicates the value of ξ . The horizontal axis is ξ . We have used a sample with size 40×10 .

Figs. 6(b5)–6(b8). It is well fitted by the function

$$|\psi_{\text{fit}}(t, x)| = A \operatorname{sech}[k_x(x - v_x t)] \quad (18)$$

as in Fig. 3(e), where parameters A , k_x , and v_x are given in its caption. This is the well-known soliton solution of the one-dimensional Schrödinger equation, although it is not a solution of the present two-dimensional model. See Appendix A.

Furthermore, the wave packet turns at a corner without backscattering or diffraction, as shown in Figs. 6(c1)–6(c8). We interpret these phenomena to mean that a chiral solitonlike edge state is formed from the topological edge modes by the nonlinear interaction. We have found that it is realized only around $\xi = 4\kappa$ in the present system.

E. Self-trapped state

We study the jump around $\xi \simeq 5.6\kappa$ in Fig. 5(a). We show the time evolution of the spatial distribution in a strong nonlinear model ($\xi = 10\kappa$) in Figs. 4(b1)–4(b5), where the state remains trapped to the initial site. To show the self-trapping transition, we calculate the amplitude at the initial site after enough time:

$$|\psi_{L_x/2, 1}|^2 \equiv \lim_{t \rightarrow \infty} |\psi_{L_x/2, 1}(t)|^2. \quad (19)$$

We show it as a function of ξ in Fig. 5(b). There is a sharp transition around $\xi \simeq 5.6\kappa$. The nonlinear-induced self-trapping transition has been discussed also in other contexts [8,43,44].

In the strong nonlinear regime ($\xi \gg 1$), we may approximate Eq. (1) as

$$i \frac{d\psi_n}{dt} = -\xi |\psi_n|^2 \psi_n, \quad (20)$$

where all equations are separated one another. The solution is

$$\psi_n(t) = r_n e^{i\theta_n(t)}, \quad (21)$$

with a constant r_n and $\theta_n = \xi r_n^2 t + c$. Hence, the amplitude does not decrease. By imposing the initial condition Eq. (11), we have $r_n = 1$ for $t = 0$, namely, the state is strictly localized at the initial site as in Fig. 3(d).

V. DISCUSSION

We studied nonlinear effects on the chiral edge state in the nonlinear Schrödinger equation. Our results would

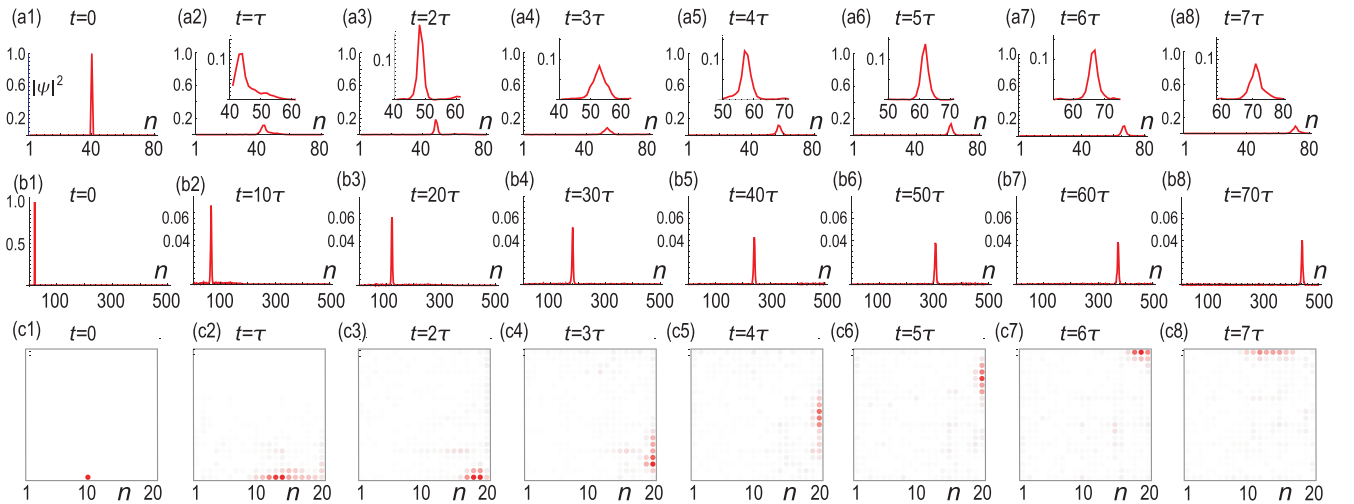


FIG. 6. Time evolution of the LDOS $|\psi_n|^2$ in the nonlinear model ($\xi = 4\kappa$). (a1)–(a8) Spatial profile of the LDOS along the edge of a rectangular sample with size 80×10 . Each inset shows an enlarged figure of a soliton. (b1)–(b8) The LDOS along the edge of a rectangular sample with size 500×10 . (c1)–(c8) The LDOS in a whole square sample with size 20×20 . A wave packet is found to turn at a corner without backscattering or diffraction. The time step is $\tau = 10$ in units of $1/\kappa$. The horizontal axis is the lattice site n .

be experimentally observed in nonlinear topological photonic systems [1–3,5–9], where the topological edge states must be directly observed by photoluminescence. It is also possible to observe the time evolution of the edge states [33,36].

Comments are in order. First, the nonlinearity parameter ξ is introduced by the Kerr effect in the case of photonics [31,32] and fixed in each sample. Nevertheless, it is enough to prepare a sample with one fixed ξ , which we explain in Appendix B. Second, it is necessary to tune $\alpha = \pi/2$ to realize the present model because the number of bands is given by $2\pi/\alpha$. The system turns into a quasicrystal when $2\pi/\alpha$ is irrational. However, it is possible to make a fine-tuning of α in optical experiments [35,36].

In this paper, we have studied a Chern insulator with two opposite chiral edges. What happens in a Chern insulator with one chiral edge is an interesting problem. A typical example is the Haldane model, which we discuss in Appendix C. As far as we have checked, no solitonlike states are formed.

ACKNOWLEDGMENTS

The author is very much grateful to N. Nagaosa for helpful discussions on the subject. This work is supported by the Grants-in-Aid for Scientific Research from MEXT KAKENHI (Grants No. JP17K05490 and No. JP18H03676). This work is also supported by CREST, JST (JPMJCR16F1 and JPMJCR20T2).

APPENDIX A: NONLINEAR SCHRÖDINGER EQUATION

The one-dimensional tight-binding nonlinear Schrödinger equation is given by Eq. (1). The corresponding continuum theory reads

$$i \frac{d\psi}{dt} + \kappa \frac{d^2\psi}{dx^2} + \xi |\psi|^2 \psi = 0. \quad (\text{A1})$$

There is an exact soliton solution given by

$$\begin{aligned} \psi(t, x) = & \sqrt{\Omega} \text{sech} \left[\sqrt{\Omega} \left(\sqrt{\frac{\xi}{2\kappa}} x - \frac{\xi v_0}{2} t \right) \right] \\ & \times \exp \left[i \sqrt{\frac{\xi}{2\kappa}} \frac{v_0 x}{2} - i \frac{\xi}{2} \left(\frac{v_0^2}{4} - \Omega \right) t \right] \end{aligned} \quad (\text{A2})$$

or

$$|\psi(t, x)| = A \text{sech}[k_x(x - v_x)t], \quad (\text{A3})$$

with

$$A = \sqrt{\Omega}, \quad k_x = \sqrt{\frac{\Omega\xi}{2\kappa}}, \quad v_x = v_0 \sqrt{\frac{\xi\kappa}{2}}. \quad (\text{A4})$$

This is the fitting function Eq. (9) in the main text, although it is not an exact solution of the present two-dimensional tight-binding model.

APPENDIX B: SCALE TRANSFORMATION

We point out that the nonlinearity strength is controlled only by changing the initial condition without changing a sample. By making a scale transformation $\psi_n = 1/\sqrt{|\xi|} \tilde{\psi}_n$, it follows from Eq. (1) that

$$i \frac{d\tilde{\psi}_n}{dt} + \kappa \sum_m M_{nm} \tilde{\psi}_m + |\tilde{\psi}_n|^2 \tilde{\psi}_n = 0, \quad (\text{B1})$$

where the nonlinearity parameter ξ is removed.

In the dynamics starting from a localized state at $(L_x/2, 1)$ under the initial condition Eq. (6) in the main text, this initial condition is transformed to

$$\tilde{\psi}_n^{\text{ini}} = \sqrt{|\xi|} \delta_{n_x, L_x/2} \delta_{n_y, 1}, \quad (\text{B2})$$

namely, the quench dynamics subject to Eq. (1) is reproduced with the use of the nonlinear Eq. (B1) with the modified initial condition Eq. (B2). Consequently, it is possible to use a single sample to investigate the quench dynamics at various

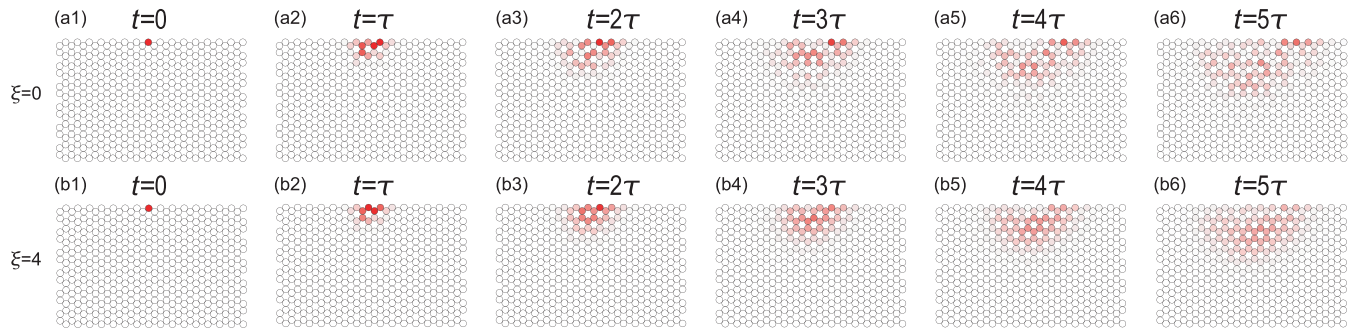


FIG. 7. Time evolution of the spatial profile of the LDOS $|\psi_n|^2$ in the Haldane model. (a) Linear model with $\xi = 0$ and (b) the nonlinear model with $\xi = 4\kappa$. The time step is $\tau = 10$ in units of $1/\kappa$. We have set $\lambda = 0.2$.

nonlinearity strength only by changing the initial condition as in Eq. (B2).

APPENDIX C: HALDANE MODEL

In the main text, we have studied the Chern insulator which has two opposite chiral edge modes. What happens if we introduce the nonlinear term in the model with one chiral edge mode is an interesting problem. The typical example is the Haldane model defined by

$$M_{\text{Haldane}} = \sum_{\langle i,j \rangle} |i\rangle\langle j| + i \frac{\lambda}{3\sqrt{3}} \sum_{\langle\langle i,j \rangle\rangle} v_{ij} |i\rangle\langle j|, \quad (\text{C1})$$

where $|i\rangle\langle j|$ represents a hopping from site j to site i in the honeycomb lattice, and $\langle i,j \rangle / \langle\langle i,j \rangle\rangle$ run over all the nearest-/next-nearest-neighbor hopping sites. The first term represents the nearest-neighbor hopping with the transfer energy and the second term represents the effective spin-orbit interaction, where $v_{ij} = +1$ if the next-nearest-neighbor hopping is anticlockwise and $v_{ij} = -1$ if it is clockwise with respect to the positive z axis.

We show the time evolution starting with the initial condition which is localized at one site in Fig. 7. The propagation of the edge modes is found to be almost insensitive to ξ .

-
- [1] D. Leykam and Y. D. Chong, *Phys. Rev. Lett.* **117**, 143901 (2016).
- [2] X. Zhou, Y. Wang, D. Leykam, and Y. D. Chong, *New J. Phys.* **19**, 095002 (2017).
- [3] L. J. Maczewsky, M. Heinrich, M. Kremer, S. K. Ivanov, M. Ehrhardt, F. Martinez, Y. V. Kartashov, V. V. Konotop, L. Torner, D. Bauer, and A. Szameit, *Science* **370**, 701 (2020).
- [4] Y. Hadad, A. B. Khanikaev, and A. Alu, *Phys. Rev. B* **93**, 155112 (2016).
- [5] D. Smirnova, D. Leykam, Y. Chong, and Y. Kivshar, *Appl. Phys. Rev.* **7**, 021306 (2020).
- [6] T. Tulous, R. W. Bomantara, C. H. Lee, and J. Gong, *Phys. Rev. B* **102**, 115411 (2020).
- [7] S. Kruk, A. Poddubny, D. Smirnova, L. Wang, A. Slobozhanyuk, A. Shorokhov, I. Kravchenko, B. Luther-Davies, and Y. Kivshar, *Nat. Nanotechnol.* **14**, 126 (2019).
- [8] M. Ezawa, *Phys. Rev. B* **104**, 235420 (2021).
- [9] M. S. Kirsch, Y. Zhang, M. Kremer, L. J. Maczewsky, S. K. Ivanov, Y. V. Kartashov, L. Torner, D. Bauer, A. Szameit, and M. Heinrich, *Nat. Phys.* **17**, 995 (2021).
- [10] M. Ezawa, *Phys. Rev. Res.* **4**, 013195 (2022).
- [11] D. D. J. M. Snee, and Y.-P. Ma, *Extreme Mech. Lett.* **30**, 100487 (2019).
- [12] P.-W. Lo, C. D. Santangelo, Bryan Gin-ge Chen, C. M. Jian, K. Roychowdhury, and M. J. Lawler, *Phys. Rev. Lett.* **127**, 076802 (2021).
- [13] M. Ezawa, *J. Phys. Soc. Jpn.* **90**, 114605 (2021).
- [14] M. Ezawa, *Phys. Rev. B* **105**, 165418 (2022).
- [15] Y. Hadad, J. C. Soric, A. B. Khanikaev, and A. Alu, *Nat. Electron.* **1**, 178 (2018).
- [16] K. Sone, Y. Ashida, and T. Sagawa, *Phys. Rev. Res.* **4**, 023211 (2022).
- [17] M. Ezawa, *J. Phys. Soc. Jpn.* **91**, 024703 (2022).
- [18] F. Zangeneh-Nejad and R. Fleury, *Phys. Rev. Lett.* **123**, 053902 (2019).
- [19] M. A. Gorlach and A. P. Slobozhanyuk, *Nanosystems: Phys. Chem. Math.* **8**, 695 (2017).
- [20] D. A. Dobrykh, A. V. Yulin, and A. P. Slobozhanyuk, A. N. Poddubny, and Y. S. Kivshar, *Phys. Rev. Lett.* **121**, 163901 (2018).
- [21] R. E. Peierls, *Proc. Phys. Soc. London* **52**, 34 (1940).
- [22] F. R. N. Nabarro, *Proc. Phys. Soc.* **59**, 256 (1947).
- [23] Y. S. Kivshar and D. K. Campbell, *Phys. Rev. E* **48**, 3077 (1993).
- [24] Y. S. Kivshar and B. A. Malomed, *Rev. Mod. Phys.* **61**, 763 (1989).
- [25] S. Mukherjee and M. C. Rechtsman, *Phys. Rev. X* **11**, 041057 (2021).
- [26] Z. Zhang, R. Wang, Y. Zhang, Y. V. Kartashov, F. Li, H. Zhong, H. Guan, K. Gao, F. Li, Y. Zhang, and M. Xiao, *Nat. Commun.* **11**, 1902 (2020).
- [27] S. K. Ivanov, Y. V. Kartashov, L. J. Maczewsky, A. Szameit, and V. V. Konotop, *Opt. Lett.* **45**, 1459 (2020).
- [28] J. C. Eilbeck, P. S. Lomdahl, and A. C. Scott, *Physica D* **16**, 318 (1985).

- [29] D. N. Christodoulides and R. I. Joseph, *Opt. Lett.* **13**, 794 (1988).
- [30] P. G. Kevrekidis, K. O. Rasmussen, and A. R. Bishop, *Int. J. Mod. Phys. B* **15**, 2833 (2001).
- [31] A. Szameit, D. Blöer, J. Burghoff, T. Schreiber, T. Pertsch, S. Nolte, A. Tünnermann, and F. Lederer, *Opt. Express* **13**, 10552 (2005).
- [32] D. N. Christodoulides, F. Lederer, and Y. Silberberg, *Nature (London)* **424**, 817 (2003).
- [33] M. A. Bandres, S. Wittek, G. Harari, M. Parto, J. Ren, M. Segev, D. N. Christodoulides, and M. Khajavikhan, *Science* **359**, 1231 (2018).
- [34] N. Korabel and G. M. Zaslavsky, *Physica A* **378**, 223 (2007).
- [35] M. Hafezi, E. Demler, M. Lukin, and J. Taylor, *Nat. Phys.* **7**, 907 (2011).
- [36] M. Hafezi, S. Mittal, J. Fan, A. Migdall, and J. Taylor, *Nat. Photonics* **7**, 1001 (2013).
- [37] G. Harari, M. A. Bandres, Y. Lumer, M. C. Rechtsman, Y. D. Chong, M. Khajavikhan, D. N. Christodoulides, and M. Segev, *Science* **359**, eaar4003 (2018).
- [38] D. J. Thouless, M. Kohmoto, M. P. Nightingale, and M. den Nijs, *Phys. Rev. Lett.* **49**, 405 (1982).
- [39] I. Dana, Y. Avron, and J. Zak, *J. Phys. C: Solid State Phys.* **18**, L679 (1985).
- [40] M. Kohmoto, *J. Phys. Soc. Jpn.* **61**, 2645 (1992).
- [41] Y. Hatsugai and M. Kohmoto, *Phys. Rev. B* **42**, 8282 (1990).
- [42] M. Kohmoto, *Phys. Rev. B* **39**, 11943 (1989).
- [43] M. Ezawa, *Phys. Rev. B* **105**, 125421 (2022).
- [44] D. Cai, A. R. Bishop, and N. Gronbech-Jensen, *Phys. Rev. Lett.* **72**, 591 (1994).